Journal of Materials Chemistry A

Accepted Manuscript

This is an *Accepted Manuscript*, which has been through the Royal Society of Chemistry peer review process and has been accepted for publication.

Accepted Manuscripts are published online shortly after acceptance, before technical editing, formatting and proof reading. Using this free service, authors can make their results available to the community, in citable form, before we publish the edited article. We will replace this *Accepted Manuscript* with the edited and formatted *Advance Article* as soon as it is available.

You can find more information about *Accepted Manuscripts* in the Information for Authors.

Please note that technical editing may introduce minor changes to the text and/or graphics, which may alter content. The journal's standard Terms & Conditions and the Ethical guidelines still apply. In no event shall the Royal Society of Chemistry be held responsible for any errors or omissions in this *Accepted Manuscript* or any consequences arising from the use of any information it contains.

ROYAL SOCIETY OF CHEMISTRY

www.rsc.org/materialsA

Journal of Materials Chemistry A

ARTICLE

Organic solvent vapor treatment of the lead iodide layer in the two-step sequential deposition of $CH_3NH_3PbI_3$-based perovskite solar cells

Received 00th January 20xx,
Accepted 00th January 20xx

DOI: 10.1039/x0xx00000x

www.rsc.org/

M. I. El-Henawey[a,b], Ryan S. Gebhardt [b,c], M. M .El-Tonsy [a] , Sumit Chaudhary[b,c]

The two step sequential deposition of $CH_3NH_3PbI_3$-based perovskite solar cells has been modified by applying toluene and chlorobenzene vapors during the preparation of the PbI_2 film leading to growth of the PbI_2 grain size. PbI_2 films treated with these solvent vapors have more surface area with which CH_3NH_3I can react leading to a more desirable perovskite layer morphology. This resulted in a significant increase in the performance of the corresponding perovskite solar cell devices where the average power conversion efficiency was enhanced from 5.2 % for the control device up to 8.4 and 10.2 % for toluene and chlorobenzene-treated devices, respectively.

1. Introduction

Obtaining electrical energy from the sun using an economical method is a radical solution for the problems of limited fossil fuels and global warming. In recent years, harnessing solar energy using the traditional solar cells based on silicon has gained tremendous traction. However, exploitation of inexhaustible solar energy is still limited, and there is a need for alternative high-efficiency low-cost solutions. The new generation of the mixed organic–inorganic halide perovskite solar cells is an exciting development in this direction. Their efficiency has recently reached nearly 20%[1-3]. The high efficiency stems from remarkable properties of $CH_3NH_3PbI_3$ such as a large absorption coefficient, small electron/hole effective masses[4], a direct band gap close to the visible region[5, 6], and large electron-hole diffusion lengths which may reach at least 100 nanometers[7]. In addition to the high photovoltaic performance of the perovskite solar cells, they are easily fabricated from four common deposition methods reported thus far: one-step solution deposition[6]; two-step sequential deposition[8]; vapor assisted solution process[9] and dual-source vapor deposition[10]. In recent years, many researchers have conducted investigations to raise the efficiency of perovskite solar cells. These investigations include the exploration of various hole-transporting materials and electron-transporting materials and understanding their impact on the device performance[11]. Although approaches such as varying the precursor molar ratios,[12] thermal annealing,[13] casting conditions[14], and using mixed solvents to produce a smooth perovskite film surface with uniform crystal domains[15] have been investigated, controlling the morphology of the perovskite film still represents one of the main challenges in the device fabrication process .One such method to control the film morphology was the solvent engineering approach presented by Jeon *et al*. where the perovskite film is deposited from a precursor solution dissolved in a mixture of dimethylsulfoxide (DMSO) and γ-butyrolactone immediately followed by a toluene drip, which leads to an extremely uniform and dense perovskite layer[16]. Xiao *et al.* used a similar approach in which they induced the crystallization of the perovskite film by dripping chlorobenzene immediately after spin coating the precursor solution. This process produced a perovskite film with a crystal size on the order of microns and yielded an average power conversion efficiency (PCE) more than 13%[17]. Another strategy to optimize the morphology of the perovskite film was by employing solvent annealing; this was demonstrated by Xiao *et al.*, who annealed the perovskite layer in the presence of dimethylformamide (DMF) vapor.

[a] *Physics Department, Faculty of Science, Mansoura University, Mansoura 35516, Egypt.*
[b] *Department of Electrical and Computer Engineering, Iowa State University, Ames, Iowa 50011, USA.*
[c] *Department of Materials Science and Engineering, Iowa State University, Ames, Iowa 50011, USA.*

Electronic Supplementary Information (ESI) available: [details of any supplementary information available should be included here]. See DOI: 10.1039/x0xx00000x

Journal of Materials Chemistry A Accepted Manuscript

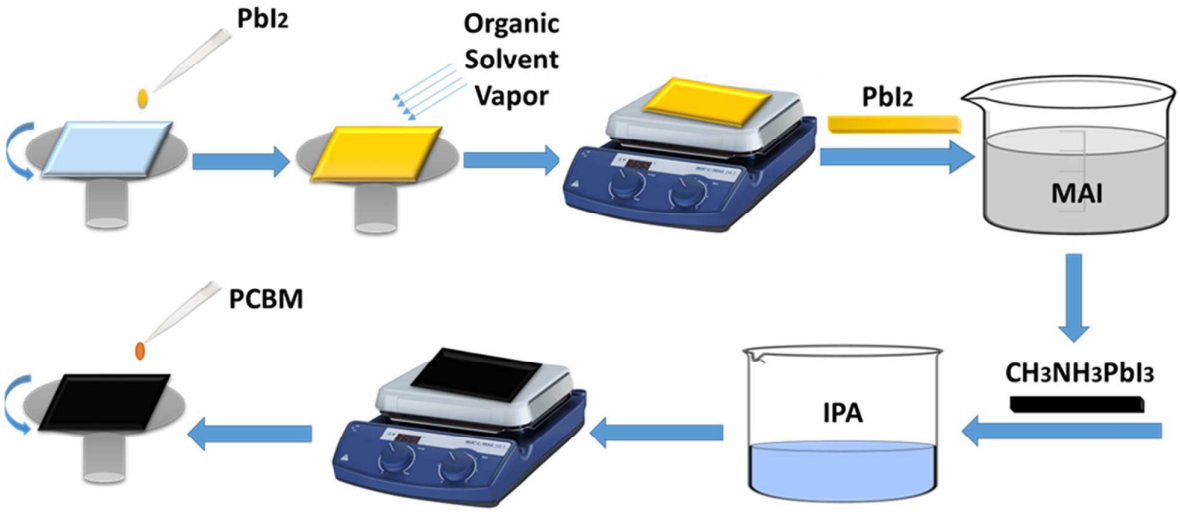

Fig. 1 Schematic illustration of our modified two-step sequential deposition method for fabricating the perovskite films where the organic solvent vapors were applied immediately after the deposition of PbI2.

Both PbI_2 and CH_3NH_3I, the precursor constituents of the perovskite layer, are highly soluble in DMF. The solvent annealing supported the diffusion and reorganization of the precursor molecules and ions leading to growth of the perovskite crystals[18]. Lian *et al.* also applied the vapors of both 1,2-dichlorobenzene (DCB) and DMSO during the second stage (i.e. application of CH_3NH_3I to PbI_2) of the perovskite film formation. They concluded that the presence of the organic solvent vapors facilitated the growth and coalescence of the grains, which illustrates the importance of the vapor environment during perovskite formation[19]. It is quite obvious from these and other previous works that improving the morphology of the perovskite film by increasing the crystal size and enhancing the crystalline quality of the grains is critical to realize high performance devices[14, 17] .

In the current work, we modified the typical two-step sequential deposition process by exposing the wet PbI_2 layer to toluene and chlorobenzene vapors. We chose toluene and chlorobenzene due to their miscibility with the host solvent DMF. We believe this method can harness effects of both solvent and thermal annealing in a single step. Toluene and chlorobenzene vapors provide a solvent annealing atmosphere, which can reduce the DMF evaporation rate and helps to promote the growth of the PbI_2 nanocrystals[20]. In addition, PbI_2 crystal growth may be assisted thermally due to heat provided by the vapor temperature of ~120°C. Our approach favorably altered the morphology of the PbI_2 layer by enhancing the growth of PbI_2 crystallites resulting in higher porosity, which is conducive for reaction with CH_3NH_3I. Resultant photovoltaic devices had higher optical absorbance and power conversion efficiency than the control devices with untreated PbI_2 layers.

2. Experimental

2.1 Materials

Devices were fabricated on fluorine doped tin oxide (FTO) coated glass substrates (Delta Technologies). Poly (3,4-ethylenedioxythiophene)-polystyrene sulfonate (PEDOT:PSS), (Clevios P VP AI 4083) was purchased from Heraeus Precious Metals GmbH & Co. KG. [6,6]-phenyl-C_{61}-butyric acid methyl ester (PCBM) was purchased from 1-materials Inc. Lead iodide (beads, -10 mesh, and 99.999% metals basis) was purchased from Alfa Aesar. Methylammonium iodide (CH_3NH_3I) was purchased from Dyesol. Anhydrous solvents N,N-dimethylformamide (DMF, 99.8%), 2-propanol (99.5%), toluene (99.8%) and chlorobenzene (99.8%) were purchased from Sigma-Aldrich. All materials were used as received.

2.2 Device Fabrication

FTO substrates were sequentially cleaned with detergent, deionized water, and 2-propanol. The substrates were blown dry with nitrogen and kept on a hot plate at 150°C for 10 min. Then, they were exposed to air plasma for 10 min. The PEDOT:PSS solution was filtered with a PVDF 0.45 µm filter and spin-coated on FTO substrates at 4000 rpm for 30 s, followed by annealing at 150°C for 20 min. Then, the substrates were transferred to an N_2-filled glovebox with oxygen and water levels less than 10 and 0.1 ppm, respectively. A 461 mg mL^{-1} solution of lead iodide (PbI_2) in DMF was spin-coated on top of the PEDOT:PSS layer at 3000 rpm for 30 s. The wet PbI_2 films were exposed to different organic solvent vapor atmospheres, N_2 (i.e. as a control), toluene, and chlorobenzene for 30 s. The toluene and chlorobenzene solvent vapors were generated by heating 2 mL of toluene or chlorobenzene in a 25 mL flask at 120°C. The solvent vapors were directed *via* a tube onto the top of the PbI_2 films. This process was followed by annealing the PbI_2 films at 90°C for 5 min. The substrates were left to cool to room temperature and then dipped into a solution of 2-propanol with 10 mg mL^{-1} CH_3NH_3I for 60 s.

Journal of Materials Chemistry A Accepted Manuscript

This journal is © The Royal Society of Chemistry 20xx

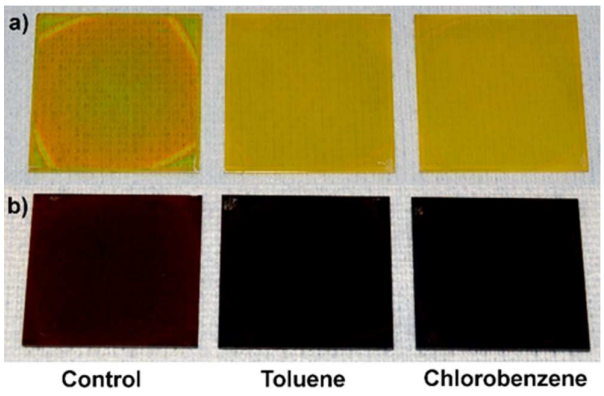

Fig. 2 Photographs of (a) FTO/PEDOT:PSS/PbI_2 films and corresponding (b) FTO/PEDOT: PSS/$CH_3NH_3PbI_3$ films.

The films were rinsed quickly with 2-propanol, followed by annealing at 90°C for 20 min to complete the crystal formation and remove any remaining solvent. A 30 mg mL^{-1} solution of PCBM in chlorobenzene was spin-coated at 1500 rpm for 60 s on the perovskite layer as the electron transport layer. Finally, 100 nm of Ag was thermally evaporated in 10^{-6} mbar vacuum on top of the PCBM layer.

2.3 Device and Thin-Film Characterization

The current-voltage characteristics were obtained using a computer-controlled Keithley 236 source meter measurement unit. One sun illumination was obtained using a light source (LS150 Abet Technologies) and calibrated with a reference crystalline silicon solar cell. External quantum efficiency (EQE) was measured using a custom setup built from a single grating monochromator (Horiba Jobin Yvon), 100 W halogen bulb (OSRAM Bellaphot), and current pre-amplifier (Ithaco, Inc.). An optical chopper (Thor Laboratories) coupled with a lock-in amplifier (Stanford Research Systems) were used to reduce noise in the system. Optical absorption/transmission was measured in a Varian Cary 5000 ultraviolet-visible-near-infrared (UV-vis-NIR) spectrophotometer. The X-ray diffraction (XRD) patterns were recorded using a Siemens D500 X-ray diffractometer. Samples were sputtered with 5 nm iridium before obtaining scanning electron microscope (SEM) images using a field emission SEM (FEI Quanta-250).

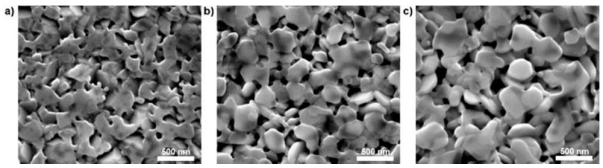

Fig. 4 The SEM micrographs of PbI_2 films exposed to different atmospheres of (a) N_2, (b) toluene vapor, and (c) chlorobenzene vapor, respectively. The scale bar is 500 nm.

3. Results and Discussion

3.1 Perovskite Formation

The schematic illustration of our modified two-step sequential deposition process is shown in Fig. 1. After the deposition of the PbI_2 layer, toluene or chlorobenzene vapor was employed to enhance the crystallization and induce growth of the PbI_2 grains. As shown in Fig. 2a, it is clear that the appearance of the PbI_2 film changes from transparent red-yellow for the control substrate (i.e. in N_2 atmosphere) to opaque dark-yellow with 30 s exposure to toluene or chlorobenzene vapor. To further investigate the changes occurring in the PbI_2 layer, we performed XRD and SEM. The XRD patterns obtained from PbI_2 films prepared under the effect of N_2, toluene vapor, and chlorobenzene vapor are shown in Fig. 3. It was found that in the cases of PbI_2 films exposed to toluene and chlorobenzene vapors, intensity of the most representative XRD peak of the PbI_2 nanocrystals at 2θ = 12.56° strongly increased and the full width at half maximum (FWHM) reduced.

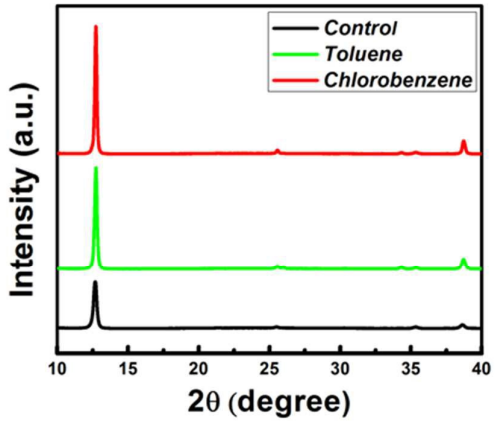

Fig. 3 The X-ray diffraction patterns of PbI_2 films fabricated in N_2, toluene, and chlorobenzene atmospheres.

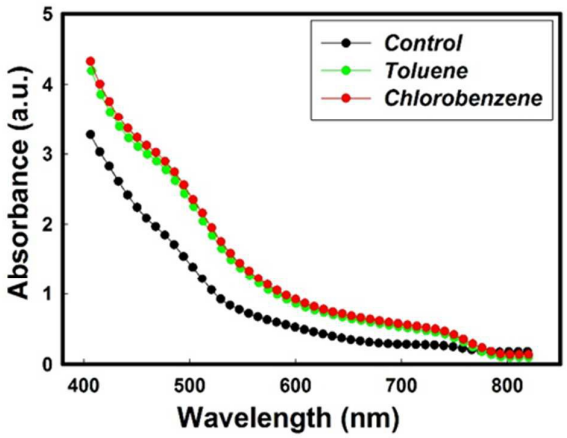

Fig. 5 Absorption spectra of perovskite films obtained from PbI_2 layers prepared under the effect of N_2, toluene vapor, and chlorobenzene

Journal of Materials Chemistry A Accepted Manuscript

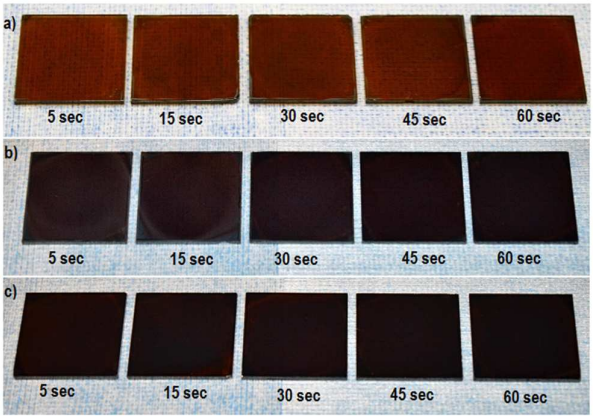

Fig. 6 Conversion of PbI_2 to perovskite with respect to dipping time for (a) control, (b) toluene, and (c) chlorobenzene samples.

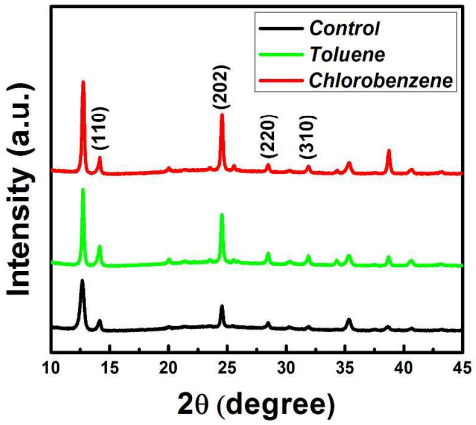

Fig. 8 The X-ray diffraction patterns of perovskite layers obtained from PbI_2 films fabricated in N_2, toluene, and chlorobenzene atmospheres.

The average grain size D of the PbI_2 nanocrystals can be estimated from the (001) peak at 12.56° using the Scherrer equation: $\boldsymbol{D = k\lambda/(\beta cos(\theta))}$ where k is the Scherrer constant (equal to 0.94), λ is the X-ray wavelength (equal to 0.154 nm), θ is the Bragg diffraction angle, and β is the FWHM of the (001) diffraction peak, respectively[21]. We found that the FWHM of the diffraction peak at 12.56° is 0.259, 0.199, and 0.159, which correspond to average PbI_2 crystal sizes of 32.2, 41.8, and 52.2 nm for the control, toluene, and chlorobenzene samples, respectively. This means that the toluene and chlorobenzene vapors enhanced the growth of PbI_2 crystals.

The SEM images of the PbI_2 films in Fig. 4 show larger domain sizes for the films treated with toluene and chlorobenzene vapors, confirming the XRD results. Enhancing the PbI_2 crystal growth was not the only benefit of toluene and chlorobenzene vapors. As is clear from the SEM images, these vapors also helped to create cavities between the PbI_2 crystals. Such cavities can enhance the penetration of CH_3NH_3I in the PbI_2 layer during dipping, leading to more complete perovskite formation. On the other hand, CH_3NH_3I diffusion into the PbI_2 layer may be hindered in the control sample, whose SEM image shows less prominent cavities. This effect is evident in the images of the perovskite films, shown in Fig. 2b, where the perovskite films changed from light-brown for the control to dark-black for the PbI_2 layers treated with toluene and chlorobenzene vapors.

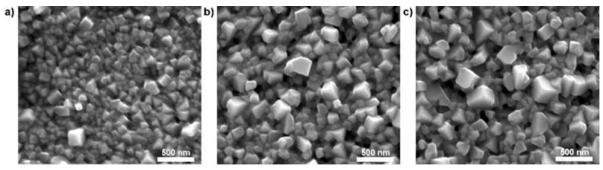

Fig. 7 The SEM micrographs of perovskite layers obtained from PbI_2 films exposed to atmospheres of (a) N_2, (b) toluene vapor, and (c) chlorobenzene vapor, respectively. The scale bar is 500 nm.

Fig. 5 shows the absorption spectra of the corresponding perovskite films. Their absorption covers a wide range of light wavelengths from the visible to the near-infrared region. It is observed that the $CH_3NH_3PbI_3$ films corresponding to the PbI_2 prepared under the influence of toluene or chlorobenzene vapor have higher absorbance, indicating that more PbI_2 is converted into $CH_3NH_3PbI_3$. These increases in absorbance of the toluene and chlorobenzene perovskite films support the claim of increased porosity (cavities) of the PbI_2 layers exposed to toluene and chlorobenzene vapors; more cavities allow CH_3NH_3I to more easily reach the interior of PbI_2, facilitating a more complete transformation to $CH_3NH_3PbI_3$.

For further investigation of the effect of the porosity on the diffusion reaction between the PbI_2 film and the CH_3NH_3I solution, we can look at the color change of the PbI_2 film with dipping time as shown in Fig. 6. It is obvious that the control sample suffers from a slow PbI_2 to perovskite conversion rate. As the dipping time is increased from 5 to 60 seconds, the color only slightly changes to light brown.

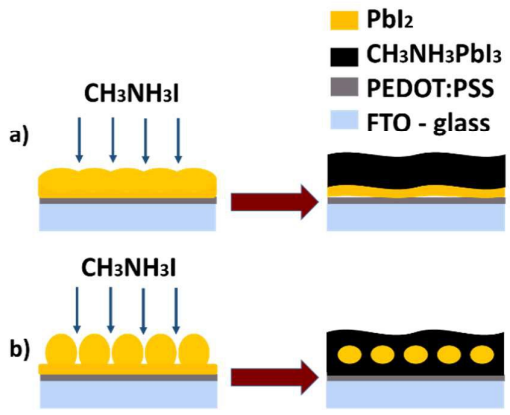

Fig. 9 Schematic illustration of the diffusion process of CH_3NH_3I through (a) compact PbI_2 layer (b) porous PbI_2 layer.

Journal of Materials Chemistry A Accepted Manuscript

This journal is © The Royal Society of Chemistry 20xx

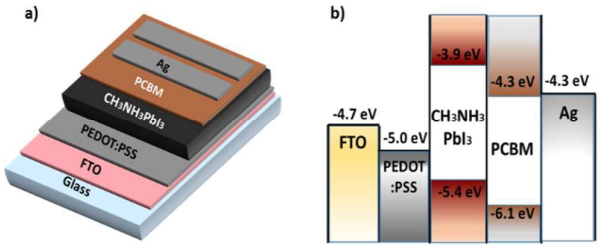

Fig. 10 (a) Device architecture. (b) Schematic energy level diagram of the FTO/PEDOT:PSS /$CH_3NH_3PbI_3$/PCBM/Ag cells.

This difficulty in the conversion of the control sample may be related to the compact nature of the PbI_2 film corresponding to this sample. In contrast, the toluene and chlorobenzene samples show a faster conversion rate and turn dark brown quickly. This supports the advantage of having a porous PbI_2 film during the fabrication of a two-step perovskite layer via dipping in CH_3NH_3I solution.

One can expect that the change in the morphology of PbI_2 films also changes the morphology of the perovskite layer. Fig. 7 shows the SEM images of the perovskite layers corresponding to the PbI_2 films exposed to N_2, toluene vapor, and chlorobenzene vapor. It is obvious that the grain size of the perovskite crystals is dependent on that of the PbI_2 crystals where the smallest PbI_2 crystals obtained from the control sample produce the smallest perovskite crystals, while the largest PbI_2 crystals resulting from the exposure to toluene and chlorobenzene vapors produce the largest perovskite crystals. To confirm existence of the $CH_3NH_3PbI_3$ crystals, we carried out XRD measurement for the perovskite layers, as shown in Fig. 8. The $CH_3NH_3PbI_3$ films show strong diffraction peaks at 2θ of 14.0°, 24.3°, 28.4° and 31.7°, which correspond to the (110), (202), (220) and (310) lattice planes of cubic $CH_3NH_3PbI_3$ crystals, respectively[22].

Interestingly, the diffraction peak at 12.56°, which is attributed to unreacted PbI_2, still shows high intensity. It has been shown that the perovskite transformation is limited by the diffusion of CH_3NH_3I into PbI_2 and unreacted PbI_2 remains in the film even after 2 hours of dipping time[20, 23]. If the PbI_2 layer is smooth, one would expect a layered structure to develop such as that shown in Fig. 9a. By increasing the porosity of the PbI_2 layer via treatment with toluene or chlorobenzene vapor, one might expect a core-shell like structure to develop as shown in Fig. 9b.

It has been reported that in a n-i-p structure (FTO/TiO_2/$CH_3NH_3PbI_3$/Spiro-OMeTAD/gold), a thin layer of PbI_2 at the perovskite – electron transport layer (TiO_2) interface can have a beneficial effect of reducing recombination[23, 24]. However, we use a p-i-n structure with PEDOT:PSS collecting holes. If there is PbI_2 present at the PEDOT:PSS/$CH_3NH_3PbI_3$ interface, it will likely hurt the device performance due to the unfavorable band alignment of PbI_2 for hole collection (conduction band minimum of -4.05 eV and valence band maximum of -6.35 eV)[23]. Therefore, we expected that the increased porosity of the PbI_2 layer caused by the toluene or chlorobenzene vapor should lead to less PbI_2 at the PEDOT:PSS/$CH_3NH_3PbI_3$ interface in the final device, and the device performance should enhance.

3.2 Device performance

It has been shown that the photovoltaic device performance is strongly dependent on the PbI_2 film morphology[25]. We also expected the morphological changes induced by toluene and chlorobenzene to improve the device performance. Fig. 10 shows the configuration and the energy level diagram of the perovskite solar cells that we fabricated[15, 26].

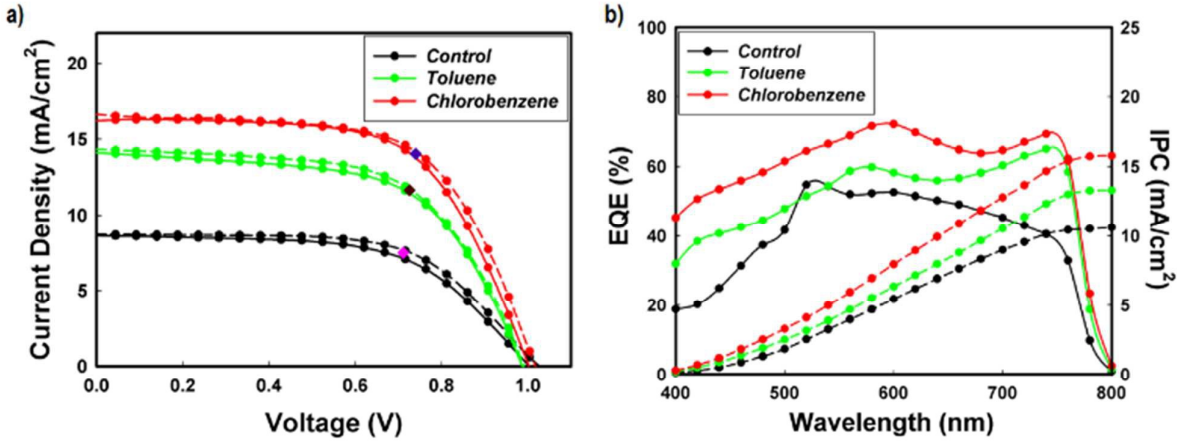

Fig. 11 (a) Current density - voltage (J–V) curves with forward (solid lines) and reverse (dashed lines) scans at 50 mV s^{-1} sweep rate. The pink, brown, and purple diamonds that lie between each two curves represents the stabilized photocurrent near the maximum power point for the control, toluene, and chlorobenzene devices, respectively, as measured by holding the devices at constant voltage under illumination for 60 sec. (b) The solid lines show the EQE spectra and the dashed lines show the corresponding integrated photocurrent (IPC).

Journal of Materials Chemistry A Accepted Manuscript

Table 1 The photovoltaic parameters for the perovskite solar cells fabricated in this study.

Sample	V_{oc} (V)		J_{sc} (mA cm^{-2})		FF (%)		PCE (%)	
	Forward	Reverse	Forward	Reverse	Forward	Reverse	Forward	Reverse
Control	0.99 ± 0.00	1.02 ± 0.00	8.5 ± 0.1	8.6 ± 0.4	60.2 ± 1.3	63.0 ± 0.8	5.1 ± 0.1	5.4 ± 0.1
Toluene	0.99 ± 0.00	0.99 ± 0.01	13.4 ± 0.9	13.7 ± 0.6	62.5 ± 0.5	62.8 ± 0.3	8.3 ± 0.5	8.6 ± 0.4
Chlorobenzene	1.00 ± 0.00	1.01 ± 0.00	16.1 ± 0.0	16.4 ± 0.0	63.4 ± 0.2	63.4 ± 1.4	10.1 ± 0.0	10.3 ± 0.1

Fig. 11a shows the current density - voltage (J-V) curves with both forward and reverse scans, and table 1 lists the photovoltaic parameters of our devices. The open-circuit voltage (V_{oc}) and the fill factor (FF) were nearly similar for all devices, but the devices treated with toluene and chlorobenzene vapors showed better photovoltaic performance than the control device due to enhancement in short-circuit current density (J_{sc}). Moreover, the toluene and chlorobenzene devices are showing slightly less hysteresis in the J-V curves compared to the control device.

Im *et al.* reported that the J_{sc} increases with increasing $CH_3NH_3PbI_3$ cuboid size and light-harvesting efficiency and charge-carrier extraction are significantly affected by the cuboid size[27]. It was reported that the larger perovskite crystals reduce the interfacial area, which can hinder charge collection, between grains. Larger grains also show lower bulk defects and higher mobility, so the photo-generated carriers can be more easily collected[14]. This may explain the increase in J_{sc} of the toluene and chlorobenzene devices, which showed a larger cuboid size than the control device. Fig. 11b shows the external quantum efficiency (EQE) of our devices. The devices that underwent toluene and chlorobenzene vapor processing show a broadband increase in EQE over the measured wavelengths. The integrated photocurrents from the EQE spectra (10.4, 13.2, and 15.7 mA/cm^2 for the control, toluene, and chlorobenzene devices, respectively) show generally good agreement with the J-V measurement. Finally, we were able to double the performance of the two-step $CH_3NH_3PbI_3$ solar cell devices by applying toluene or chlorobenzene vapor during the preparation of the PbI_2 layer for only 30 seconds, significantly shorter time than typically required by solvent annealing approaches[20].

Conclusions

In summary, we studied the effects of applying different organic solvent vapors on the PbI_2 films during the typical two-step fabrication of $CH_3NH_3PbI_3$ perovskite solar cells. We observed that the PbI_2 grain size, as well as the film porosity, increased with exposure to toluene and chlorobenzene vapors. The increased porosity allowed the CH_3NH_3I to more easily penetrate the PbI_2 film leading to a more complete PbI_2 to perovskite transformation with larger grains. These changes resulted in the enhancement of the absorbance and up to 10.2% photovoltaic power conversion efficiency, which was about 97 % higher than the control device.

Acknowledgements

Mohamed EL-Henawey would like to thank the fellowship support from the Egyptian government under Contract JS3067.

Notes and references

1. M. A. Green, A. Ho-Baillie and H. J. Snaith, *Nature Photonics*, 2014, **8**, 506-514.
2. H. J. Snaith, *The Journal of Physical Chemistry Letters*, 2013, **4**, 3623-3630.
3. I. Deretzis, A. Alberti, G. Pellegrino, E. Smecca, F. Giannazzo, N. Sakai, T. Miyasaka and A. La Magna, *Applied Physics Letters*, 2015, **106**, 131904.
4. A. Filippetti and A. Mattoni, *Physical Review B*, 2014, **89**.
5. P. Umari, E. Mosconi and F. De Angelis, *Sci Rep*, 2014, **4**, 4467.
6. H. S. Kim, C. R. Lee, J. H. Im, K. B. Lee, T. Moehl, A. Marchioro, S. J. Moon, R. Humphry-Baker, J. H. Yum, J. E. Moser, M. Gratzel and N. G. Park, *Sci Rep*, 2012, **2**, 591.
7. G. Xing, N. Mathews, S. Sun, S. S. Lim, Y. M. Lam, M. Gratzel, S. Mhaisalkar and T. C. Sum, *Science*, 2013, **342**, 344-347.
8. J. Burschka, N. Pellet, S. J. Moon, R. Humphry-Baker, P. Gao, M. K. Nazeeruddin and M. Gratzel, *Nature*, 2013, **499**, 316-319.
9. Q. Chen, H. Zhou, Z. Hong, S. Luo, H. S. Duan, H. H. Wang, Y. Liu, G. Li and Y. Yang, *J Am Chem Soc*, 2014, **136**, 622-625.
10. M. Liu, M. B. Johnston and H. J. Snaith, *Nature*, 2013, **501**, 395-398.
11. T. Salim, S. Sun, Y. Abe, A. Krishna, A. C. Grimsdale and Y. M. Lam, *J. Mater. Chem. A*, 2015, **3**, 8943-8969.
12. Q. Wang, Y. Shao, Q. Dong, Z. Xiao, Y. Yuan and J. Huang, *Energy Environ. Sci.*, 2014, **7**, 2359-2365.
13. A. Dualeh, N. Tétreault, T. Moehl, P. Gao, M. K. Nazeeruddin and M. Grätzel, *Advanced Functional Materials*, 2014, **24**, 3250-3258.
14. W. Nie, H. Tsai, R. Asadpour, J.-C. Blancon, A. J. Neukirch, G. Gupta, J. J. Crochet, M. Chhowalla, S. Tretiak and M. A. Alam, *Science*, 2015, **347**, 522-525.
15. H. B. Kim, H. Choi, J. Jeong, S. Kim, B. Walker, S. Song and J. Y. Kim, *Nanoscale*, 2014, **6**, 6679-6683.

Journal of Materials Chemistry A Accepted Manuscript

This journal is © The Royal Society of Chemistry 20xx

16. N. J. Jeon, J. H. Noh, Y. C. Kim, W. S. Yang, S. Ryu and S. I. Seok, *Nat Mater*, 2014, **13**, 897-903.
17. M. Xiao, F. Huang, W. Huang, Y. Dkhissi, Y. Zhu, J. Etheridge, A. Gray-Weale, U. Bach, Y. B. Cheng and L. Spiccia, *Angew Chem Int Ed Engl*, 2014, **53**, 9898-9903.
18. Z. Xiao, Q. Dong, C. Bi, Y. Shao, Y. Yuan and J. Huang, *Adv Mater*, 2014, **26**, 6503-6509.
19. J. Lian, Q. Wang, Y. Yuan, Y. Shao and J. Huang, *J. Mater. Chem. A*, 2015, **3**, 9146-9151.
20. J. Song, E. Zheng, J. Bian, X.-F. Wang, W. Tian, Y. Sanehira and T. Miyasaka, *J. Mater. Chem. A*, 2015, **3**, 10837-10844.
21. U. Holzwarth and N. Gibson, *Nat Nanotechnol*, 2011, **6**, 534.
22. C.-H. Chiang, Z.-L. Tseng and C.-G. Wu, *J. Mater. Chem. A*, 2014, **2**, 15897-15903.
23. D. H. Cao, C. C. Stoumpos, C. D. Malliakas, M. J. Katz, O. K. Farha, J. T. Hupp and M. G. Kanatzidis, *APL Materials*, 2014, **2**, 091101.
24. Q. Chen, H. Zhou, T. B. Song, S. Luo, Z. Hong, H. S. Duan, L. Dou, Y. Liu and Y. Yang, *Nano Lett*, 2014, **14**, 4158-4163.
25. K. Hwang, Y. S. Jung, Y. J. Heo, F. H. Scholes, S. E. Watkins, J. Subbiah, D. J. Jones, D. Y. Kim and D. Vak, *Adv Mater*, 2015, **27**, 1241-1247.
26. W. Chen, Y. Wu, J. Liu, C. Qin, X. Yang, A. Islam, Y.-B. Cheng and L. Han, *Energy Environ. Sci.*, 2015, **8**, 629-640.
27. J. H. Im, I. H. Jang, N. Pellet, M. Gratzel and N. G. Park, *Nat Nanotechnol*, 2014, **9**, 927-932.

Journal of Materials Chemistry A Accepted Manuscript